JACS
JOURNAL OF THE AMERICAN CHEMICAL SOCIETY

Article

pubs.acs.org/JACS

Correlated Electrochemical and Optical Detection Reveals the Chemical Reactivity of Individual Silver Nanoparticles

Vitor Brasiliense,[†] Anisha N. Patel,[†] Ariadna Martinez-Marrades,[‡] Jian Shi,[§] Yong Chen,[§] Catherine Combellas,[†] Gilles Tessier,[*,‡] and Frédéric Kanoufi[*,†]

[†]Sorbonne Paris Cité, Université Paris Diderot, Interfaces, Traitements, Organisation et Dynamique des Systèmes, CNRS-UMR 7086, 15 rue J. A. Baif, F-75013 Paris, France

[‡]Sorbonne Paris Cité, Université Paris Descartes, Neurophotonics Laboratory, CNRS-UMR 8250, 45 rue des Saints-Pères, F-75006 Paris, France

[§]Chemistry Department, Ecole Normale Supérieure-PSL Research University CNRS-UMR 8640, 24 Rue Lhomond, F-75005 Paris, France

Supporting Information

ABSTRACT: Electrochemical (EC) impacts of single nanoparticles (NPs) on an ultramicroelectrode are coupled with optics to identify chemical processes at the level of individual NPs. While the EC signals characterize the charge transfer process, the optical monitoring gives a complementary picture of the transport and chemical transformation of the NPs. This is illustrated in the case of electrodissolution of Ag NPs. In the simplest case, the optically monitored dissolution of individual NPs is synchronized with individual EC spikes. Optics then validates *in situ* the concept of EC nanoimpacts for sizing and counting of NPs. Chemical complexity is introduced by using a precipitating agent, SCN^-, which tunes the overall electrodissolution kinetics. Particularly, the charge transfer and dissolution steps occur sequentially as the synchronicity between the EC and optical signals is lost. This demonstrates the level of complexity that can be revealed from such electrochemistry/optics coupling.

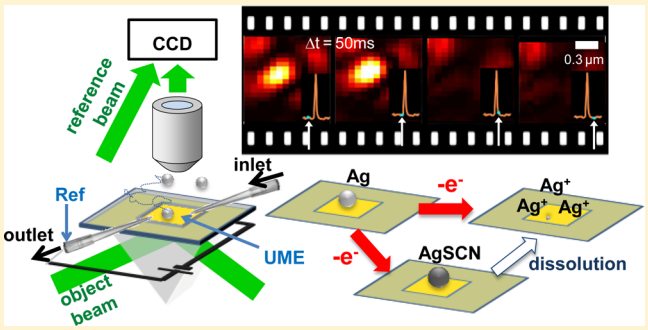

INTRODUCTION

Over the past few decades, technological advances have allowed a steady decrease in the size of the smallest entities that can be studied. Indeed, nanoparticles (NPs) have been developed in virtually all branches of science. Most studies are, however, achieved over large ensembles of NPs, whereas NPs' special properties often rely on their individual behaviors. It therefore becomes imperative to understand the chemistry of individual NPs. Silver NPs, in particular, are extensively used due to their antimicrobial properties, which essentially rely on their ability to controllably dissolve and deliver Ag^+ ions.[1] The mechanism of Ag NPs' dissolution is driven not only by their oxidation but also, owing to the affinity of Ag^+ for various anions, by the chemical environment of the NPs. A challenge in the control and understanding of the reactivity of antimicrobial agents is to observe the action of a single antimicrobial agent, e.g., a single Ag NP, directed toward a single bacterial agent. It is crucial to be able to address the chemical transformation of individual Ag NPs *in situ*. The highest spatial resolutions are provided by environmental transmission electron microscopy (TEM); however, this is far from being used routinely,[2] and highly ionizing beams are strongly invasive in terms of NPs chemistry. A powerful and simple alternative is provided by nanoelectrochemistry, through the time-resolved analysis of stochastic collisions of individual NPs on ultramicroelectrodes (UMEs),[3,4] or from nanoconfined electrochemical (EC) cells.[5] Although such EC nanoimpact experiments provide, *in situ*, much valuable information concerning the electron transfer process associated with the NP impact, they fail to fully characterize the associated chemical processes. Examples of phenomena invisible to electrochemistry alone include partial oxidation, slow dissolution kinetics, and chemical or phase transformation. To resolve these situations requires correlating EC signals to complementary *in situ* visualization of the process.[2,6−12]

This study demonstrates, for the first time, the simultaneous EC and optical visualization of individual nanoimpact events of Ag NPs on an UME. This approach delivers a complete picture of the electrodissolution process, i.e., visualization of the electron transfer through individual EC nanoimpact signatures, while the associated chemical (dissolution) process is monitored at individual NPs by 3D superlocalization optical microscopy. Indeed, optical microscopies—such as surface plasmon resonance (SPR),[9] dark-field imaging,[10] holography,[11]

Received: December 17, 2015
Published: February 22, 2016

DOI: 10.1021/jacs.5b13217
J. Am. Chem. Soc. 2016, 138, 3478−3483

and fluorescence imaging[7,8,12]—have recently emerged to image electrodes under operation and consequently study EC processes at individual domains of micrometer[7] or nanometer[8] (NPs, vesicles) sizes. Most studies focused on reactive processes occurring within the limited field of view of the optical systems: within <2 μm from the electrode,[7,8,10,12] or within the range of the evanescent wave, <200 nm, for SPR imaging.[9] However, the third dimension is also essential: holography[11] provides the possibility to measure particle−surface distances and analyze particle movements and size while chemical processes unfold over a large volume (typically 100 × 100 × 30 μm^3). With 50 mW dark-field laser illumination, particles down to 10 nm can be detected,[13] which is comparable to SPR sensitivities.[9] In the context of NP electrochemistry,[11b] the third dimension provided by holography allows *in situ* size analysis, evidencing a diffusiophoretic transport mode of NPs, triggered by electrochemical actuation, or distinguishing between the dissolution and the departure of the NP from the electrode. These works also set quantitative grounds for holography-based estimates of individual NP dissolution rates from the time-evolution of the optical signals (the intensity of light scattered by individual NPs). However, while optical methods allow visualizing individual particles, they have rarely[7] been associated with complementary detection of individual EC events.

An UME working as a low-current detector and enabling optical monitoring is mandatory to provide both optical and EC individual signatures. By using microfabricated semi-transparent gold UMEs (see Figure 1), we are now able to record the current impact for the oxidation of individual Ag NPs at the same time as optically monitoring, in 3D by holographic microscopy,[14] the NP properties. In addition to the correlation between two signatures, we take advantage of the complementary methods to visualize two different steps: the electron transfer step, from the EC signature, and its associated chemical step (dissolution) from the optics. It is exemplified in the case of the electrodissolution in the absence or presence of complexing (or precipitating) agents, here SCN^- anions, allowing the tuning of the dynamics of the dissolution step. Indeed, precipitating anions may slow down (SCN^-)[11b] or retard (Cl^-)[11a] NPs' dissolution by tens of seconds after their ensemble oxidation. Here, the overall electrodissolution mechanism is recorded by coupled EC and optical signals at the single NP level. In this respect, this work also extends to the *in situ* monitoring of the transformation of individual Ag NPs into AgSCN NPs or, more generally, to phase transformation processes such as electrocrystallization.[2]

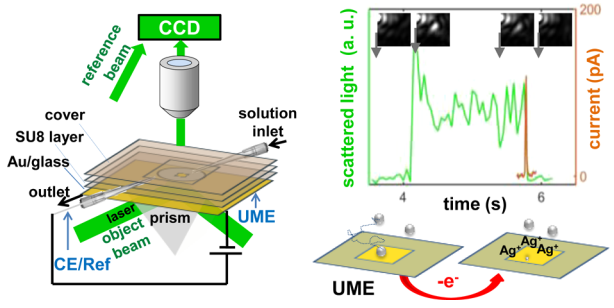

Figure 1. Set-up and EC fluidic device used for combined optical 3D localization and EC detection of Ag NPs' impacts on a Au UME. Green: example of the light scattered by an individual Ag NP (measured at the center of the 2 × 2 μm^2 inset 2D images of the UME plane) during its landing in the UME plane (rapid increase of the scattered light), and its disappearance correlated to a current spike (brown) associated with its electrodissolution in KNO_3.

EXPERIMENTAL SECTION

Chemicals. Colloidal solutions of Ag NPs (50 nm radius, citrate stabilized) were obtained from Sigma-Aldrich. Their size distribution was characterized by dynamic light scattering (DLS, Zetasizer 3000HS, Malvern Instruments). All aqueous solutions were prepared using ultrapure water of resistivity not less than 18.2 MΩ·cm. The colloidal electrolytic solutions were prepared just before use. All reagents were of analytical grade from Sigma-Aldrich.

UME Fabrication Procedure. The transparent UMEs are fabricated by lithography. The full process (see Supporting Information (SI), Figure SI 1) takes place in a clean room. The transparent gold electrode was obtained from glass slides (Figure SI 1, 1.). After surface cleaning with isopropanol, a 5 nm titanium adhesion layer and a 40 nm gold layer were deposited on the glass slide using a K675XD turbo sputter-coater (Quorum Technologies). Next, a 10 μm thick layer of photosensitive resin (SU8-3010) was spin-coated at 3000 rpm for 60 s over the electrode (Figure SI 1, 2.). Following a soft baking at 65°C for 1 min and 95°C for 3 min, the resist layer was exposed to UV light (Hamamatsu) through a chrome mask for 15 s at 13 mW/cm^2. The chrome mask contained a 50 × 50 μm^2 square, defined by a μPG101 laser writer (Heidelberg Instruments). The insolated resin was post-baked at 65 °C for 1 min and 95 °C for 2 min. These steps yield the resin cross-linking, making it insoluble in the developer. Finally, the resist was developed, for a few seconds, in a bath of SU8 developer (Microchem) so that only the unexposed parts of the SU8 film were removed, thus creating a gold window (Figure SI 1, 3.). The microfluidic cell was finally assembled using a spacer, ca. 100 μm thick, and cell delimiter, cut out from parafilm, micropipetes as inlet/outlet for the solution, and a glass coverslip to close the cell (Figure SI 1, 4.). The Ag quasi-reference electrode (QRE) was inserted in the outlet after the cell was filled with the solution. EC nanoimpact experiments, without optical monitoring, were also performed at standard 25 μm diameter Pt disk UME obtained from Pt wire embedded in glass, as reported in the literature.[3,4] Electrochemical measurements were performed with a CH 760E bipotentiostat (CH Instruments, IJ Cambria).

RESULTS AND DISCUSSION

Ag NP Electrodissolution in KNO_3. The active area, 50 × 50 μm^2, of an Au UME was defined from SU8 photoresist lithography on an Au-coated microscope glass slide (Figure 1). It is also the size of the optical field of view, so that the whole UME in contact with the solution is monitored optically by a 100× objective. The UME is then built into a microfluidic cell, of ~10 × 5 × 0.1 mm^3 volume, provided with micropipettes and an Ag wire serving as both AgQRE and counter electrode for EC measurement.

We first address the correlation between individual optical and EC collisions when the electrodissolution of Ag NPs is performed under fast conditions. This is obtained in KNO_3 (or in excess of SCN^-, as will be seen later). A 0.18 pM colloidal solution of 50 nm Ag NPs in 0.05 M KNO_3 supporting electrolyte was injected into the microfluidic EC cell containing the transparent UME. NPs subjected to Brownian motion eventually reach the UME surface that is polarized at a potential positive enough to ensure diffusion-controlled NP oxidation and dissolution (typically 0.6−0.9 V vs AgQRE), while the current is monitored over time. As described in Compton's work,[3] every time a NP is oxidized at the UME surface, a current spike is recorded, corresponding to its electrodissolution,

DOI: 10.1021/jacs.5b13217
J. Am. Chem. Soc. 2016, 138, 3478−3483

$$Ag \rightarrow Ag^{+} + e^{-} \quad (1)$$

from which the charge, Q, and therefore the NP size (here an EC radius, denoted r_{EC}) can be inferred from Faraday's law,

$$Q = \frac{4}{3}\pi\frac{\rho F}{M}r_{EC}^{3} \quad (2)$$

with ρ and M respectively the NP density and molecular mass.

If, at the same time, microscopy is used to record the light scattered by individual NPs, their position can be deduced from the 3D superlocalization of the diffraction pattern representing the NP in the holograms. From each hologram, a 2D image of the light scattered by individual NPs can also be reconstructed in the different planes illuminated and explored by holography. For better visualization, SI Movies 1 and 2, and the different images discussed herein, are 2D images reconstructed in a given plane. More specifically, during the monitoring of the electrochemical process, the presented data are obtained in the plane of the UME. In these images, light-scattering objects, such as Ag NPs, are seen as bright diffraction or Airy patterns, of apparent size ca. 0.6 μm. We have previously shown, using numerical simulations, that the plasmonic resonance of Ag NPs is modified when they are in the vicinity of a thin Au layer,[11b] so that the light scattered by the NP contacting the UME, I_{sc}, scales with the volume of the NP. Then, by recording the variation of I_{sc}, the variation of the NP volume is inferred, giving a complementary and independent monitoring of the NP dissolution step.

Two scenarios have been monitored: NPs already present on the UME surface before polarization and NPs arriving at the UME surface during their Brownian movement; the latter scenario corresponds to the EC nanoimpact concept. SI Movie 1 is a 2D movie, slowed down 4 times, showing the holographic reconstruction of an 8.2 × 16.4 μm^2 region of the Au UME plane. This 2D optical monitoring presents the movement of an individual Ag NP during such an EC nanoimpact. The NP is wandering around in the vicinity of the UME surface until it finally makes contact (nearby a scattering defect) and, ca. 1.5 s later, disappears. The green trace in Figure 1 (right) summarizes the behavior of this very NP. It corresponds to the time evolution of the light recorded in this reconstructed plane of the UME, at the pixel position where the NP lands and eventually disappears (see zoomed-in images from Movie 1 in the inset of Figure 1, right, and in Figure SI 2). Along with this optical signal, the EC signal is recorded (brown), also evidencing an EC impact on the UME. The EC spike coincides with the final optical disappearance of the NP, in agreement with its electrodissolution and not with its landing. As the entire surface of the UME is scrutinized optically, both techniques are unambiguously monitoring the same phenomena.

For each of the NPs oxidized (N = 13), whichever the situation, pre-adsorbed or colliding NPs, the optical dissolved volume coincides with the detection of the EC spike. The EC charge exchanged (5.4 pC in Figure 1) also corresponds to the theoretical total oxidation (total dissolution) of an Ag NP of r_{EC} = 52 nm. The values of r_{EC} for N = 13 EC nanoimpacts agree with the size distribution of the NP solution (obtained from DLS, see SI, section III). Whenever possible, for NPs which were freely moving before their impact with the UME, the NP hydrodynamic radius, r_H, inferred from mean-square displacement (MSD) analysis, convincingly corroborates these measurements of r_{EC} (examples in SI, section IV).

Figures 2 (left) and SI 3 exemplify the other type of situation encountered: a NP that arrived on the UME before its

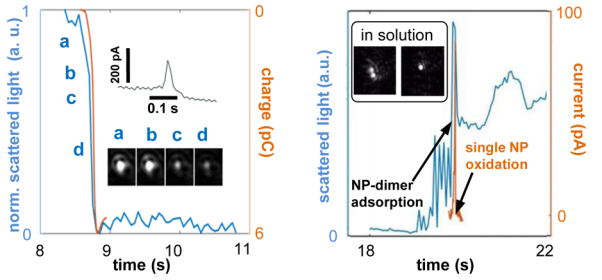

Figure 2. Correlated EC and optical signals for Ag NPs' electrodissolution in KNO_3. (Left) Comparison between the total exchanged charge (brown) and the scattered optical intensity (blue). Inset: oxidation peak and temporal evolution of 2 × 2.7 μm^2 reconstructed images of the plane of the UME (intervals τ = 50 ms). (Right) Agglomerate formation and oxidation: in solution, two NPs are merging into an agglomerate (5.6 × 6.4 μm^2 reconstructed planes in the solution) that then adsorbs on the UME (t = 20 s). Upon oxidation (current in brown), the optical intensity at the arrival pixel (blue) drops to half its value.

polarization disappears ca. 8.7 s after the polarization began. Here again, an EC signal is recorded concomitantly with the optical disappearance of the NP (evidenced from the successively recorded 2 × 2.7 μm^2 reconstructed images of the UME plane shown as the inset of Figure 2, left). As the exchanged EC charge and the optical intensity are two independent measures of the NP volume, both signals (onset and kinetics) are expected to overlap, as in Figure 2.

This study in KNO_3, or in the absence of precipitating agent, shows conclusively that the dissolution of Ag NPs is concomitant with their oxidation that may not take place immediately upon landing: NPs remain for a certain period of time in the vicinity of the surface and stochastically oxidize. This stochasticity is rather surprising and can be due to a number of reasons. For instance, the UME might be partially active, and the particle might have landed over a non-electroactive site of the UME. In this case, the residence time would relate to a target-search strategy[15] in which the diffusion time required until a reactive site of the UME is found may be quite long. Indeed, the diffusion of NPs in solution is generally hindered near walls, such as the UME surface, and a decrease of the diffusion by at least 1 order of magnitude is expected.[16] It is also likely that this near-wall hindered diffusion freezes the NP within <10 nm of the UME. If the position of individual NPs can be monitored by holography with ultimate 3 × 3 × 10 nm^3 precision,[14] a NP in contact with the UME or within 10 nm of the UME cannot be differentiated by 3D super-resolution holography. This is currently under investigation.

Monitoring Agglomerate. Another advantage of the 3D optical control is its ability to monitor reactivity at the level of NP agglomerates. Even though this corresponds to rare individual events, Figures 2 (right) and SI 4a show the agglomeration of two NPs in solution: the NPs are approaching each other until, even though optically resolved, i.e., separated by >0.7 μm, they start interacting during a few frames before merging together into a NP dimer. The agglomerate formation is corroborated by the tracking of its trajectory, whose corresponding MSD analysis (Figure SI 9) reveals a diffusion coefficient significantly smaller than that of a single 50 nm NP (3.1 vs 4.8 $\mu m^2/s$). This diffusion coefficient corresponds to an

DOI: 10.1021/jacs.5b13217
J. Am. Chem. Soc. 2016, 138, 3478−3483

agglomerate of apparent r_H = 70 nm (SI, section IV), compatible with a NP dimer agglomerate.

Later on, the same agglomerate hits the UME. The optical signature recorded at the pixel where the agglomerate collides with the surface is presented in Figures 2 (right, blue) and SI 4b, along with the EC impact (brown) recorded at the UME. The latter EC impact indicates that the agglomerate is not fully oxidized, as the charge estimated from the impact corresponds to r_{EC} = 50 nm, i.e., that of a single NP. Such partial dissolution of the agglomerate is corroborated by the optical trace, which shows that some optically scattering material is still left on the electrode surface; I_{sc} decreases by a factor of 2, also consistent with the dissolution of a single 50 nm NP. This strongly confirms the EC signature on the basis of the fact that only one NP from the initial NP dimer agglomerate remains after a single NP dissolution step. This indicates that NP agglomerates do not behave electrochemically as larger particles, especially if the electrical contact between the NPs within the agglomerate is inefficient. Such coupled monitoring, at the level of individual entities, provides evidence for previous theories of incomplete agglomerate oxidation, related to either loss of contact between NPs upon dissolution (and NP escape in bulk) or deactivation of NPs due to the capping agent.[17] Optical monitoring leans in favor of the latter route.

While a few groups have studied individual NPs via EC impacts or by optical methods, this is the first time that both are performed simultaneously, allowing the observation of a correlation between charge injection and NP dissolution, i.e., the chemical process. In the scope of NP chemistry, it provides insights into the dissolution mechanism at the individual NP level and/or into the chemical processes associated with the ET step.

Ag NP Electrodissolution in KSCN. To illustrate the potentialities of our setup for unraveling chemical processes, we have introduced chemical complexity into the dissolution process. Anions such as SCN^-, acting as precipitating and/or complexing agents, may influence the Ag NP oxidation. As a result, at low [SCN^-], a product of low solubility, $AgSCN_s$, should be formed with Ag^+. The oxidation of the Ag NP is then expected to produce a $AgSCN_s$ NP (eq 3) before it is dissolved (eq 4) (with $0 \le x \le 3$, see SI, section VI).

$$Ag + SCN^- \rightarrow AgSCN_s + e^- \quad (3)$$

$$AgSCN_s + xSCN^- \rightarrow Ag(SCN)_{x+1}^{x-} \quad (4)$$

At high [SCN^-], soluble complexes with higher degrees of ligands are formed ($Ag(SCN)_2^-$, $Ag(SCN)_3^{2-}$, $Ag(SCN)_4^{3-}$). Therefore, [SCN^-] allows the tuning of the dissolution of $AgSCN_s$ and, in turn, the chemistry associated with Ag NPs' oxidation. The latter was then performed with different [SCN^-] and, as before, under sufficiently high potential (typically ca. 0.7 V vs AgQRE), enforcing the whole process to be diffusion-controlled. The experimental results are summarized in Figure 3.

At high SCN^- concentration ([SCN^-] = 300 mM), EC nanoimpacts show that the electrodissolution process is equivalent to that observed in the absence of SCN^-. As reported by Tao,[9b] the dissolution is fast, and even if its kinetics cannot be accurately obtained from our present CCD camera frequency, the characteristic time of the charge injection is ca. 0.1 s from EC impacts. It is suggested that at this concentration, the NP is dissolved as soon as the charge is injected; formally, the electrodissolution (eqs 3 and 4) is equivalent to eq 1.

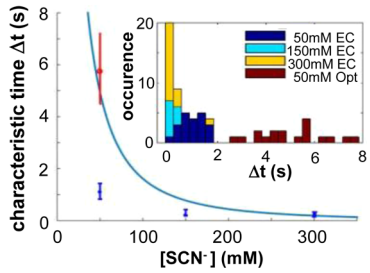

Figure 3. Dissolution (red) and charge injection (blue) times of individual Ag NPs, compared with diffusion model (line from eq 5, and see SI, section VI). Inset: histogram of the characteristic individual times (peak durations) for EC impacts in 50, 150, and 300 mM KSCN; brown bars show the duration of the dissolution monitored optically in 50 mM KSCN (see Figure 4, left).

Here it also means that the $AgSCN_s$ solid phase, if it exists, is continuously dissolved while being formed. Particularly, the characteristic dissolution time, Δt, of a NP of radiur r may be obtained, assuming a simple diffusion-reaction process, from[11b]

$$\Delta t = \frac{r^2 \rho [Ag^+]^0}{2MD_{Ag} \ln(2)} \quad (5)$$

taking into account the diffusion, D_{Ag}, of Ag^+ species in solution; $[Ag^+]^0$ corresponds to the concentration, at the NP–solution interface, of the soluble Ag^+ species and depends on [SCN^-] and the complexation equilibria (see SI, section VI).

Equation 5 predicts the evolution of the dissolution time, Δt, estimated from the optical disappearance of the NP with decreasing [SCN^-] (see SI, section VI). Δt is plotted as a polynomial line in Figure 3. Particularly, from 300 to 50 mM SCN^-, Δt is predicted to significantly increase by almost 2 orders of magnitude from, 0.1 s to ca. 4–7 s. As demonstrated in KNO_3, the optical monitoring allows a visualization of the dissolution process at the level of individual NPs. Different examples of individual Ag NP electrodissolution profiles in a 50 mM KSCN solution are given in Figures 4 (left) and SI 10. It is

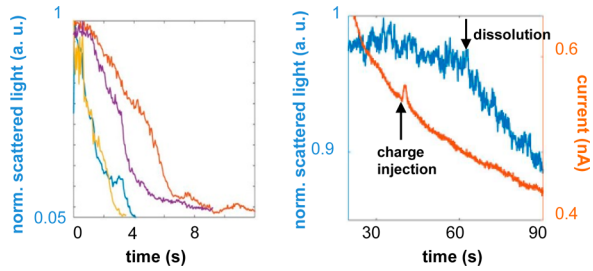

Figure 4. Oxidation of Ag NPs in 50 mM KSCN. (Left) Optical intensity profiles of four individual dissolving NPs. (Right) Correlation between optical scattered intensity (blue) and EC oxidation (brown) for a 0.18 pM Ag NP solution. The charge injection finishing before the onset of dissolution suggests eqs 3 and 4 are sequential.

worth mentioning that the large dispersion in optical data are explained by the difficulty of defining sharply a dissolution time, as the intensity may decrease in a non-trivial way, with changing slopes. In order to compare different optical intensity curves, Δt was estimated by considering only the sharp decreasing slopes, such as those shown in Figure 4 (left). The values of individual NPs' dissolution times obtained from the optical data (N = 18)

DOI: 10.1021/jacs.5b13217
J. Am. Chem. Soc. 2016, 138, 3478–3483

agree with previous results,[11b] and the average optical Δt agrees with the values predicted from eq 5. They are indeed longer than several seconds.

As above, the coupling with individual EC nanoimpacts allows inspection of the charge injection process (eq 3) preceding this dissolution step (eq 4). In a typical example (Figure 4, right, Movie 2, and SI, section III), a current spike is observed, suggesting that an Ag NP has been oxidized. However, even though both optical and EC acquisitions are triggered simultaneously, the optical change (blue) of the NP, obtained from image analysis of Movie 2, showing an 8.9 × 10.6 μm^2 section of the UME, indicates that the onset of a NP dissolution seems delayed by several seconds from the current spike associated with the individual NP's oxidation (brown). This current spike is also much broader and of lower intensity than at higher concentration (or in NO_3^-, see Figure 1, right). The following scenario was reproduced for N = 10 EC spikes, which were found associated with NPs optical disappearances: (i) the characteristic duration of the EC spikes is 1−2 s, and (ii) a time lag, of variable duration, is also observed between the EC spike and the onset of the optical disappearance. By integration, the charge of the spike (14 pC, r_{EC} = 70 nm), as of all the recorded spikes (N = 10, Figure SI 6), is consistent with the size distribution of the NPs. The EC spikes suggest the Ag NPs are completely oxidized, although in a less obvious way since, as opposed to observations in KNO_3 solution, the dissolution (eq 4) is not synchronized to the oxidation step (eq 3). These results illustrate the advantages of the coupled individual optical−electrochemical monitorings, as they each report complementary events: the individual electrochemical nanoimpacts characterize the charge transfer process, while the individual optical monitoring characterizes the dissolution (chemical) process.

To validate these results, EC nanoimpact experiments were performed at higher acquisition frequency and current resolution at a Pt UME (without optical coupling, under Faraday cage shielding) for $[SCN^-]$ = 50 mM. They confirmed the opto-EC results, as 1−2 s long oxidation times (N = 21, Figure 3) are detected with associated charge also in agreement with both the opto-EC results and the NP size distribution (see Figures SI 6 and SI 11). The characteristic EC time is then a direct estimate of the slow electrocrystallization process depicted by (eq 3). The mechanism proposed for such solid-phase transformation is intricate. If the growth of a solid phase on another one is generally initiated from defects sites,[2,18] the latter may be rare on a nanometer size surface, as was demonstrated during atomic force microscopy (AFM) monitoring of Ag growth on Pt nanoelectrodes.[6b] Moreover, the growth of these crystals is also an intricate succession of dissolution (Ag into Ag^+) and precipitation ($AgSCN_s$) steps from a supersaturated solution.[19] It is expected that the supersaturation is higher in the region of the Ag NP closer to the UME, suggesting that the precipitation (eq 3) will preferentially occur from the UME surface. Both the low conductivity of $AgSCN_s$ and the low diffusivity ($<10^{-11}$ cm^2/s) of ions in Ag-based ionic crystals may explain the observed slow and complex electrocrystallization process (eq 3). However, as the EC signal is not associated with any clear change of the optical signal, a deeper analysis of the electrocrystallization mechanism would be speculative until *in situ* AFM[6] or TEM[2] can be performed.

NPs Solution Titration from Events Frequency. Finally, the optical monitoring also allows an estimate of the conservation of the number of Ag NPs at the UME during the whole electrodissolution process. Indeed, during the course of 700 s of successive experiments in 50 mM KSCN, the optical monitoring shows that a total of 22 NPs impacted the UME and 22 disappeared, while 10 EC impacts were resolved. In the absence of convective or phoretic transport yielding flux enhancement,[5,11b,20] the frequency f of NPs' arrival to an UME was rationalized from the expression of the NP diffusive flux, with diffusion coefficient D_{NP}, toward the UME.[3,4] For a disk UME of radius a, this frequency f is given by eq 6—or similar expressions (see SI, section VIII) computed for different proper UME geometries.

$$f = 4D_{NP}[NP]a \tag{6}$$

This flux extression allowed in seminal EC nanoimpact works[3,4a] a direct estimate of the solution concentration of NPs, [NP], from the frequency of EC nanoimpacts. However, there is now convincing evidence that eq 6 does not always model the experimentally observed frequency of NPs landing on an UME.[4c,21] A possible explanation is that every nanoimpact may not result in a measurable EC signal. A recent alternative strategy proposed recording the time of first contact with the UME.[21] The alternative strategy, proposed here, directly counts, through optical monitoring, all the individual NPs landing on the UME or disappearing (desorption or dissolution) from it. This strategy is in line with the one published very recently (during the evaluation of this work), counting the attachment on a SPR-active surface of larger and highly concentrated particles.[22] The holographic observation of a smaller and much more diluted solution of Ag NPs, *in operando*, during their electrochemical oxidation is described here. The landing and disappearance of N = 22 NPs from the UME within 700 s yields frequencies of optically detected impact or disappearance $f \approx 0.03$ Hz. Assuming an average NP size of 50 nm (average NP diffusion coefficient D_{NP} = 4.8 $\mu m^2/s$), SI, eq S13, computed for the UME of this work, yields [NP] ≈ 0.15 pM, in agreement within errors (e.g., from the chosen value of D_{NP}) with the experimental value of 0.18 pM. This particularly validates the use of flux expressions such as eq 6 for estimating NP concentrations, provided that all the events are really resolved. In this case, it is then justified to consider that eq 6 equivalently applies to EC nanoimpact experiments, and therefore to consider this EC nanoimpact strategy for titration of NPs.

CONCLUSION

In conclusion, we demonstrate here the usefulness of the real-time and *in situ* optical monitoring of the whole electroactive region of an UME operating as a detector in EC nanoimpact experiments. It is illustrated in the electrodissolution of single Ag NPs. When the dissolution process is facilitated, the EC signature of oxidation of an individual NP is strictly correlated to the optical disappearance of the same individual NP. The optical monitoring also reveals events which may not be electrochemically detected. For example, in the case of NP agglomerates, the formation of a NP dimer was monitored. The subsequent landing of the dimer on the UME was observed and associated with a partial oxidation (from both the charge and optical images), suggesting that the NPs were poorly electrically connected. Optical monitoring is therefore a more precise means for the detection of events of landing or detachment processes. In particular, we have shown that the equation relating the frequency of such rare events to diffusional flux of

DOI: 10.1021/jacs.5b13217
J. Am. Chem. Soc. 2016, 138, 3478−3483

NP, and therefore allowing the titration of diluted NP solutions,[21] is valid. The access to two independent measures is also a considerable advantage when more complex or slower processes are encountered: while fast charge transfer rates are readily resolved by EC nanoimpacts, slow NP dissolution or complex chemical phase transformations are easier to follow using optics. In the case of Ag NP oxidation in a SCN^- solution, the charge injection and the dissolution steps occur sequentially. A slow electrocrystallization or solid transformation ($Ag \rightarrow AgSCN_s$) is electrochemically identified and is followed by a slower dissolution (of the $AgSCN_s$ NP), which is detected optically. This combination of techniques allows for the first identification of different chemical processes at the level of individual NPs. This highlights the diversity of chemical processes that can be encountered during single NPs chemistry and demonstrates the level of complexity that can be revealed from EC-optics coupling.

■ ASSOCIATED CONTENT

Supporting Information

The Supporting Information is available free of charge on the ACS Publications website at DOI: 10.1021/jacs.5b13217.

Movie 1, electrodissolution in KNO_3 (AVI)
Movie 2, electrodissolution in 50 mM KSCN (AVI)
Additional experimental details; description and sequence images from Movies 1 and 2; mean square displacement analysis; NP distribution (DLS, EC impacts); scattered light profiles during dissolution in KSCN; dissolution time expression and effect of SCN^-; frequency of impacts at a square UME (PDF)

■ AUTHOR INFORMATION

Corresponding Authors

*gilles.tessier@parisdescartes.fr
*frederic.kanoufi@univ-paris-diderot.fr

Notes

The authors declare no competing financial interest.

■ ACKNOWLEDGMENTS

This work was supported by Université Paris Diderot, CNRS, Agence Nationale de la Recherche (NEOCASTIP ANR-CE09-0015-01), and Laboratoire d'Excellence Institut Pierre-Gilles de Gennes pour la Microfluidique (Labex IPGG), "Investissements d'avenir" program (ANR-10-IDEX-0001-02 PSL and ANR-10-LABX-31). A.N.P. thanks Labex IPGG for funding.

■ REFERENCES

(1) (a) Morones, J. R.; Elechiguerra, J. L.; Camacho, A.; Holt, K.; Khouri, J. B..; Ramirez, J. T.; Yacaman, M. J. *Nanotechnology* **2005**, *16*, 2346−2353. (b) Shrivastava, S.; Bera, T.; Roy, A.; Singh, G.; Ramachandrarao, P.; Dash, D. *Nanotechnology* **2007**, *18*, 225103.

(2) Radisic, A.; Vereecken, P. M.; Hannon, J. B.; Searson, P. C.; Ross, F. M. *Nano Lett.* **2006**, *6*, 238−242.

(3) (a) Zhou, Y.; Rees, N.; Compton, R. G. *Angew. Chem., Int. Ed.* **2011**, *50*, 4219−4221. (b) Stuart, E. J.; Zhou, Y.; Rees, N. V.; Compton, R. G. *RSC Adv.* **2012**, *2*, 6879−6884. (c) Stuart, E. J. E.; Tschulik, K.; Omanovic, D.; Cullen, J. T.; Jurkschat, K.; Crossley, A.; Compton, R. G. *Nanotechnology* **2013**, *24*, 444002.

(4) (a) Xiao, X.; Bard, A. J. *J. Am. Chem. Soc.* **2007**, *129*, 9610−9612. (b) Dick, J. E.; Renault, C.; Bard, A. J. *J. Am. Chem. Soc.* **2015**, *137*, 8376−8379. (c) Kleijn, S. E. F.; Lai, S. C. S.; Koper, M. T. M.; Unwin, P. R. *Angew. Chem., Int. Ed.* **2014**, *53*, 3558−3586.

(5) Kang, M.; Perry, D.; Kim, Y.; Colburn, A. W.; Lazenby, R. A.; Unwin, P. R. *J. Am. Chem. Soc.* **2015**, *137*, 10902−10905.

(6) (a) Sun, T.; Yu, Y.; Zacher, B. J.; Mirkin, M. V. *Angew. Chem., Int. Ed.* **2014**, *53*, 14120−14123. (b) Velmurugan, J.; Noël, J.-M.; Nogala, W.; Mirkin, M. V. *Chem. Sci.* **2012**, *3*, 3307−3314.

(7) Fosdick, S. E.; Anderson, M. J.; Nettleton, E. G.; Crooks, R. M. *J. Am. Chem. Soc.* **2013**, *135*, 5994−5997.

(8) Meunier, A.; Jouannot, O.; Fulcrand, R.; Fanget, I.; Bretou, M.; Karatekin, E.; Arbault, S.; Guille, M.; Darchen, F.; Lemaître, F.; Amatore, C. *Angew. Chem., Int. Ed.* **2011**, *50*, 5081−5084.

(9) (a) Shan, X.; Diez-Perez, I.; Wang, L.; Wiktor, P.; Gu, Y.; Zhang, L.; Wang, W.; Lu, J.; Wang, S.; Gong, Q.; Li, J.; Tao, N. *Nat. Nanotechnol.* **2012**, *7*, 668−672. (b) Fang, Y.; Wang, W.; Wo, X.; Luo, Y.; Yin, S.; Wang, Y.; Shan, X.; Tao, N. *J. Am. Chem. Soc.* **2014**, *136*, 12584−12587.

(10) Hill, C. M.; Pan, S. *J. Am. Chem. Soc.* **2013**, *135*, 17250−17253.

(11) (a) Batchelor-McAuley, C.; Martinez-Marrades, A.; Tschulik, K.; Patel, A. N.; Combellas, C.; Kanoufi, F.; Tessier, G.; Compton, R. G. *Chem. Phys. Lett.* **2014**, *597*, 20−25. (b) Patel, A. N.; Martinez-Marrades, A.; Brasiliense, V.; Koshelev, D.; Besbes, M.; Kuszelewicz, R.; Combellas, C.; Tessier, G.; Kanoufi, F. *Nano Lett.* **2015**, *15*, 6454−6463.

(12) Hill, C. M.; Bennet, R.; Zhou, C.; Street, S.; Zheng, J.; Pan, S. *J. Phys. Chem. C* **2015**, *119*, 6760−6768.

(13) Absil, E.; Tessier, G.; Gross, M.; Atlan, M.; Warnasooriya, N.; Suck, S.; Coppey-Moisan, M.; Fournier, D. *Opt. Express* **2010**, *18*, 780−786.

(14) Martinez-Marrades, A.; Rupprecht, J. F.; Gross, M.; Tessier, G. *Opt. Express* **2014**, *22*, 29191−29203.

(15) Bénichou, O.; Loverdo, C.; Moreau, M.; Voituriez, R. *Phys. Chem. Chem. Phys.* **2008**, *10*, 7059−7072.

(16) Katelhon, E.; Compton, R. G. *Chem. Sci.* **2014**, *5*, 4592.

(17) Cloake, S. J.; Toh, H. S.; Lee, P. T.; Salter, C.; Johnston, C.; Compton, R. G. *ChemistryOpen* **2015**, *4*, 22−26.

(18) Gunawardena, G.; Hills, G.; Montenegro, I.; Scharifker, B. *J. Electroanal. Chem. Interfacial Electrochem.* **1982**, *138*, 225−232.

(19) Burton, W. K.; Cabrera, N.; Frank, F. C. *Philos. Trans. R. Soc., A* **1951**, *243*, 299−358.

(20) (a) Quinn, B. M.; van't Hof, P. G.; Lemay, S. G. *J. Am. Chem. Soc.* **2004**, *126*, 8360−8361. (b) Boika, A.; Thorgaard, S. N.; Bard, A. J. *J. Phys. Chem. B* **2013**, *117*, 4371−4380.

(21) Boika, A.; Bard, A. J. *Anal. Chem.* **2015**, *87*, 4341−4346.

(22) Wo, X.; Li, Z.; Jiang, Y.; Su, Y.-W.; Wang, W.; Tao, N. *Anal. Chem.* **2016**, *88*, 2380−2385.

DOI: 10.1021/jacs.5b13217
J. Am. Chem. Soc. 2016, 138, 3478−3483